CREX- and PREX-II-motivated relativistic interactions and their implications for the bulk properties of nuclear matter and neutron stars

Mukul Kumar [1,*] Sunil Kumar [1] Virender Thakur [1,†] Raj Kumar [1,‡] B. K. Agrawal [2,§] and Shashi K. Dhiman [1,3,¶]

[1]*Department of Physics, Himachal Pradesh University, Shimla-171005, India*
[2]*Saha Institute of Nuclear Physics, 1/AF Bidhannagar, Kolkata 700064, India*
[3]*School of Applied Sciences, Himachal Pradesh Technical University, Hamirpur-177001, India*

We investigate the implications of parity-violating electron scattering experiment on neutron skin thickness of ^{48}Ca [calcium radius experiment (CREX)] and ^{208}Pb [lead radius experiment (PREX-II)] data on the bulk properties of finite nuclei, nuclear matter, and neutron stars. The neutron skin thickness from the CREX and PREX-II data is employed to constrain the parameters of relativistic mean-field models which includes different nonlinear, self- and cross-couplings among isoscalar-scalar σ, isoscalar-vector ω, isovector-scalar δ, and isovector-vector ρ meson fields up to the quartic order. Three parametrizations of RMF model are proposed by fitting CREX, PREX-II, and both CREX as well as PREX-II data to assess their implications. A covariance analysis is performed to assess the theoretical uncertainties of model parameters and nuclear matter observables along with correlations among them. The RMF model parametrization obtained with the CREX data acquires much smaller value of symmetry energy ($J = 28.97 \pm 0.99$ MeV) and its slope parameter ($L = 30.61 \pm 6.74$ MeV) in comparison to those obtained with PREX-II data. The neutron star properties are studied by employing the equations of state composed of nucleons and leptons in β equilibrium.

I. INTRODUCTION

The nuclear equation of state (EoS) plays a vital role for understanding the properties of strongly interacting many-body systems like atomic nuclei and neutron stars [1–3]. The nuclear symmetry energy and its density dependence are key features of nuclear EoS. Constraining the density dependence of symmetry energy represents a long-standing and unresolved question in nuclear physics and astrophysics [3]. The density dependence of the symmetry energy has implications in a variety of phenomena such as heavy-ion collisions, core-collapse supernovas, and neutron-star structures. Although important, this quantity cannot be directly measured in the laboratory, it can only be derived from theories and thus to constrain their values it is necessary to identify and use relevant observables on finite nuclei. A neutron star is a highly dense and asymmetric nuclear system that has a central density of about five to six times the nuclear saturation density [4]. The study of the neutron star proclaims that its internal structure is more complex as new degrees of freedom like hyperons and quarks appear in the core. The properties of the neutron star like mass, radius, and tidal deformability can be explained by taking into account the interaction between nucleons and the mesonic degree of freedom in the form of

Lagrangian. This provides an EoS which is the main input for the calculation of neutron star properties. The several relativistic mean-field (RMF) models having effective Lagrangian density consisting of nonlinear σ, ω, ρ, and δ terms and cross terms have been analyzed for nucleonic matter and nucleonic along with hyperonic matter and accosted with the constraints of nuclear matter properties and astrophysical observations of compact star masses [5–7]. The nuclear theory studies [8–10] are mainly focusing on understanding the dense matter in compact stars (CS). The constraints on EoS at high density are imposed with accurate information of a neutron star's maximum mass and radius [1,11,12]. The precise measurement of masses of millisecond pulsars such as PSR J1614-2230 [13] and PSR J0348+0432 [14] show that the maximum mass of the neutron star should be around 2 $M\odot$. The recent observations with LIGO and Virgo of GW170817 event [15,16] of Binary Neutron Stars merger and the discovery of CS with masses around $2M_{\odot}$ [13,14,17–20] have intensified the interest in these intriguing objects. The analysis of GW170817 has demonstrated the potential of gravitational wave (GW) observations to yield new information relating to the limits on CS tidal deformability.

The recent precise parity-violating electron scattering experiments on ^{48}Ca [calcium radius experiment (CREX)] [21] and ^{208}Pb [lead radius experiment (PREX-II)] [22] provide new insights into the neutron skin thickness of nuclei. These experiments are helpful in determining the nuclear weak charge form factor by measuring the parity-violating asymmetry. The weak charge form factor has a strong correlation with the density dependence of symmetry energy and neutron skin thickness of nuclei and plays an important role in

*mukulpathania120495@gmail.com
†virenthakur2154@gmail.com
‡raj.phy@gmail.com
§sinp.bijay@gmail.com
¶shashi.dhiman@gmail.com

probing the isovector channels of energy density functionals. The parity-violating electron scattering experiments give precise and model-independent data for the nuclear weak charge form factor that can be used to constrain the energy density functionals [23]. The weak charge form factors of ^{48}Ca and ^{208}Pb reported by CREX and PREX-II experiments and their measured parity-violating asymmetry has been analyzed using density functionals and reached on a conclusion that it is difficult to describe parity-violating asymmetry simultaneously in both nuclei [24,25]. The CREX has recently given a model-independent extraction of neutron skin thickness of ^{48}Ca as $\Delta r_{np} = 0.121 \pm 0.026$ fm [21] which suggests softness of density dependence of symmetry energy. The PREX has recently given a model-independent extraction of neutron skin thickness of ^{208}Pb as $\Delta r_{np} = 0.283 \pm 0.071$ fm [22] by combining the original PREX result with the new PREX-II. The Δr_{np} has been identified as an ideal probe on symmetry energy— a key but poorly known quantity that describes the isospin dependence of EoS of nuclear matter and plays a crucial role in various issues in nuclear physics and astrophysics. The neutron skin thickness of the lead nucleus exhibits a strong positive linear correlation with the slope of symmetry energy (L) at saturation density. The value of L around the saturation density strongly affects the mass-radius relation and tidal deformability (Λ) of a neutron star and provides a unique bridge between atomic nuclei and neutron star. The large value of $\Delta r_{np} = 0.283 \pm 0.071$ fm suggests a very stiff EoS and large value of L around saturation density and generally gives rise to a large value of neutron star radius and the tidal deformability [26]. The upper limit on $\Lambda_{1.4} \leqslant 580$ for GW170817 requires softer EoS and hence softer symmetry energy coefficient [15]. The heaviest neutron star $2.14^{+0.10}_{-0.09} M_{\odot}$ of PSRJ0740+6620 [27] also limits the EoS for symmetric nuclear matter (SNM). The flow data from heavy ion collisions suggests that the EoS for SNM should be relatively softer [28].

The motivation of the present work is to generate three new relativistic interactions for the Lagrangian density of the RMF model to investigate the effect of CREX and PREX-II data on neutron skin thickness for ^{48}Ca and ^{208}Pb nuclei on the bulk nuclear properties and observed astrophysical constraints on neutron stars. A covariance analysis can also be performed to assess the theoretical uncertainties of model parameters and nuclear matter observables along with correlations among them.

The paper is organized as follows, in Sec. II, a brief outline of the RMF Lagrangian, equations of motion, and EoS for neutron stars is provided. In Sec. III, the procedure for optimization of the model parameters and covariance analysis is discussed. Numerical results and detailed discussions features of model parametrizations, finite nuclei, bulk nuclear matter, neutron star matter, and correlations among nuclear matter observables and model parameters are presented in Sec. IV. Finally, we give a summary in Sec. V.

II. THEORETICAL MODEL

The Lagrangian density for the RMF model used in the present work is based upon different nonlinear, self- and inter-couplings among isoscalar-scalar σ, isoscalar-vector ω_μ,

isovector-scalar δ, and isovector-vector ρ_μ meson fields and nucleonic Dirac field Ψ [5–7,29], is given by

$$
\begin{aligned}
\mathcal{L} = \sum_B \overline{\Psi}_B \Bigg[& i\gamma^\mu \partial_\mu - (M_B - g_{\sigma B}\sigma - g_{\delta B}\delta \cdot \tau_3) - \Bigg(g_{\omega B}\gamma^\mu \omega_\mu \\
& + \frac{1}{2} g_{\rho B}\gamma^\mu \tau_B . \rho_\mu \Bigg) \Bigg] \Psi_B + \frac{1}{2}\big(\partial_\mu \sigma \partial^\mu \sigma - m_\sigma^2 \sigma^2\big) \\
& - \frac{\overline{\kappa}}{3!} g_{\sigma N}^3 \sigma^3 - \frac{\overline{\lambda}}{4!} g_{\sigma N}^4 \sigma^4 - \frac{1}{4}\omega_{\mu\nu}\omega^{\mu\nu} + \frac{1}{2} m_\omega^2 \omega_\mu \omega^\mu \\
& + \frac{1}{4!}\zeta g_{\omega N}^4 (\omega_\mu \omega^\mu)^2 - \frac{1}{4}\rho_{\mu\nu}\rho^{\mu\nu} + \frac{1}{2} m_\rho^2 \rho_\mu \rho^\mu \\
& + \frac{1}{2}\big(\partial_\mu \delta \partial^\mu \delta - m_\delta^2 \delta^2\big) + \frac{1}{2}\Lambda_{\omega\rho} g_{\omega N}^2 g_{\rho N}^2 \omega_\mu \omega^\mu \rho_\mu \rho^\mu \\
& - \frac{1}{4}F_{\mu\nu}F^{\mu\nu} - \sum_B e\overline{\Psi}_B \gamma_\mu \frac{1+\tau_{3B}}{2} A_\mu \Psi_B \\
& + \sum_{\ell=e,\mu} \overline{\Psi}_\ell \big(i\gamma^\mu \partial_\mu - M_\ell\big)\Psi_\ell.
\end{aligned} \tag{1}
$$

The equation of motion for baryons, mesons, and photons can be derived from the Lagrangian density defined in Eq. (1). The equation of motion for baryons can be given as

$$
\begin{aligned}
\Bigg[\gamma^\mu \Bigg(i\partial_\mu - g_{\omega B}\omega_\mu - \frac{1}{2} g_{\rho B}\tau_B . \rho_\mu - e\frac{1+\tau_{3B}}{2} A_\mu \Bigg) \\
- (M_B - g_{\sigma B}\sigma - g_{\delta B}\delta \cdot \tau_3) \Bigg] \Psi_B = \epsilon_B \Psi_B.
\end{aligned} \tag{2}
$$

The Euler-Lagrange equations for the ground-state expectation values of the meson fields are

$$
\big(-\Delta + m_\sigma^2\big)\sigma = \sum_B g_{\sigma B}\rho_{sB} - \frac{\overline{\kappa}}{2} g_{\sigma N}^3 \sigma^2 - \frac{\overline{\lambda}}{6} g_{\sigma N}^4 \sigma^3, \tag{3}
$$

$$
\big(-\Delta + m_\omega^2\big)\omega = \sum_B g_{\omega B}\rho_B - \frac{\zeta}{6} g_{\omega N}^4 \omega^3 \\
- \Lambda_{\omega\rho} g_{\omega N}^2 g_{\rho N}^2 \omega\rho^2, \tag{4}
$$

$$
\big(-\Delta + m_\rho^2\big)\rho = \sum_B g_{\rho B}\tau_{3B}\rho_B - \frac{\xi}{6} g_{\rho N}^4 \rho^3 \\
- \Lambda_{\omega\rho} g_{\omega N}^2 g_{\rho N}^2 \omega^2 \rho, \tag{5}
$$

$$
\big(-\Delta + m_\delta^2\big)\delta = \sum_B g_{\delta B}\rho_{s3B} \tag{6}
$$

$$
-\Delta A_0 = e\rho_p, \tag{7}
$$

where the baryon vector density ρ_B, scalar density ρ_{sB}, and charge density ρ_p are, respectively,

$$
\rho_B = \langle \overline{\Psi}_B \gamma^0 \Psi_B \rangle = \frac{\gamma k_B^3}{6\pi^2}, \tag{8}
$$

$$
\rho_{sB} = \langle \overline{\Psi}_B \Psi_B \rangle = \frac{\gamma}{(2\pi)^3} \int_0^{k_B} d^3k \frac{M_B^*}{\sqrt{k^2 + M_B^{*2}}}, \tag{9}
$$

$$
\rho_p = \left\langle \overline{\Psi}_B \gamma^0 \frac{1+\tau_{3B}}{2}\Psi_B \right\rangle, \tag{10}
$$

with γ the spin-isospin degeneracy. The Dirac effective mass for the neutron and proton can be written as

$$M_p^* = (M - g_\sigma \sigma - g_\delta \delta),$$ (11)

$$M_n^* = (M - g_\sigma \sigma + g_\delta \delta).$$ (12)

Following the Euler-Lagrange formalism one can readily find the expressions for energy density $\mathcal{E}$ and pressure P as a function of density from Eq. (1) [30].

The energy density of the uniform matter within the framework of the RMF model is given by

$$
\begin{aligned}
\mathcal{E} = &\sum_{j=B,\ell} \frac{1}{\pi^2} \int_0^{k_j} k^2 \sqrt{k^2 + M_j^{*2}} \, dk \\
&+ \sum_B g_{\omega B} \omega \rho_B + \sum_B g_{\rho B} \tau_{3B} \rho_B \rho + \frac{1}{2} m_\sigma^2 \sigma^2 \\
&+ \frac{\kappa}{6} g_{\sigma N}^3 \sigma^3 + \frac{\overline{\lambda}}{24} g_{\sigma N}^4 \sigma^4 - \frac{\zeta}{24} g_{\omega N}^4 \omega^4 \\
&- \frac{\xi}{24} g_{\rho N}^4 \rho^4 - \frac{1}{2} m_\omega^2 \omega^2 - \frac{1}{2} m_\rho^2 \rho^2 \\
&- \frac{1}{2} \Lambda_{\omega\rho} g_{\omega N}^2 g_{\rho N}^2 \omega^2 \rho^2 + \frac{1}{2} m_\delta^2 \delta^2.
\end{aligned}
$$ (13)

The pressure of the uniform matter is given by

$$
\begin{aligned}
P = &\sum_{j=B,\ell} \frac{1}{3\pi^2} \int_0^{k_j} \frac{k^4 dk}{\sqrt{k^2 + M_j^{*2}}} - \frac{1}{2} m_\sigma^2 \sigma^2 \\
&- \frac{\overline{\kappa}}{6} g_{\sigma N}^3 \sigma^3 - \frac{\overline{\lambda}}{24} g_{\sigma N}^4 \sigma^4 + \frac{\zeta}{24} g_{\omega N}^4 \omega^4 \\
&+ \frac{\xi}{24} g_{\rho N}^4 \rho^4 + \frac{1}{2} m_\omega^2 \omega^2 + \frac{1}{2} m_\rho^2 \rho^2 \\
&+ \frac{1}{2} \Lambda_{\omega\rho} g_{\omega N}^2 g_{\rho N}^2 \omega^2 \rho^2 - \frac{1}{2} m_\delta^2 \delta^2.
\end{aligned}
$$ (14)

Here, the sum is taken over nucleons and leptons.

III. OPTIMIZATION AND COVARIANCE ANALYSIS

The optimization of the parameters (**p**) appearing in the Lagrangian [Eq. (1)] has been performed by using the simulated annealing method (SAM) [31,32] by following χ^2 minimization procedure which is given as

$$\chi^2(\mathbf{p}) = \frac{1}{N_d - N_p} \sum_{i=1}^{N_d} \left(\frac{M_i^{\exp} - M_i^{\mathrm{th}}}{\sigma_i} \right)^2,$$ (15)

where N_d is the number of experimental data points and N_p is the number of fitted parameters. The σ_i denotes adopted errors [33] and $M_i^{\exp}$ and M_i^{th} are the experimental and the corresponding theoretical values, respectively, for a given observable. The minimum value of χ_0^2 corresponds to the optimal values $\mathbf{p}_0$ of the parameters. After the optimization of the energy density functional, it is important to explore the richness of the covariance analysis. It enables one to calculate the statistical uncertainties/errors on model parameters or any calculated physical observables. The covariance analysis also provides additional information about the sensitivity of the

parameters to the physical observables, and interdependence among the parameters [33–36]. Having obtained the parameter set, the correlation coefficient between two quantities Y and Z can be calculated by covariance analysis [33,35–38] as

$$c_{YZ} = \frac{\overline{\Delta Y \Delta Z}}{\sqrt{\overline{\Delta Y^2} \ \overline{\Delta Z^2}}},$$ (16)

where covariance between Y and Z is expressed as

$$\overline{\Delta Y \Delta Z} = \sum_{\alpha\beta} \left(\frac{\partial Y}{\partial p_\alpha} \right)_{\mathbf{p}_0} C_{\alpha\beta}^{-1} \left(\frac{\partial Z}{\partial p_\beta} \right)_{\mathbf{p}_0}.$$ (17)

Here, $C_{\alpha\beta}^{-1}$ is an element of inverted curvature matrix given by

$$C_{\alpha\beta} = \frac{1}{2} \left(\frac{\partial^2 \chi^2(\mathbf{p})}{\partial p_\alpha \partial p_\beta} \right)_{\mathbf{p}_0}.$$ (18)

The standard deviation, $\overline{\Delta Y^2}$, in Y can be computed using Eq. (17) by substituting $Z = Y$.

IV. RESULTS AND DISCUSSION

We obtain parametrizations for RMF models by employing CREX, PREX-II, and combined CREX + PREX-II data by following the procedure discussed in Sec. III. The model parametrizations obtained are then used to calculate the properties of finite nuclei, infinite nuclear matter and neutron stars. We also discuss the correlations among nuclear matter observables and model parameters.

A. Parametrizations of RMF model

In the present study, three new relativistic interactions BSRV-CREX, BSRV-PREX, and BSRV-CPREX have been generated for the Lagrangian density given by Eq. (1) to investigate the effect of CREX and PREX-II data on neutron skin thickness for ^{48}Ca and ^{208}Pb nuclei on the properties of finite nuclei and neutron star matter. The parameters of the BSRV-CREX, BSRV-PREX, and BSRV-CPREX models are obtained by fitting exactly the available experimental data of Ref. [39] on binding energies (BE) and charge rms radii (r_{ch}) [40] of some closed/open-shell nuclei ^{16,24}O, ^{40,48}Ca, ^{56,68,78}Ni, ^{88}Sr, ^{90}Zr, ^{100,116,132}Sn, ^{144}Sm, and ^{208}Pb. In addition, we also include in our fit the value of neutron skin thickness for ^{48}Ca and ^{208}Pb nuclei, which is a very important physical observable to constrain the value of L that determines the linear dependence of symmetry energy.

The BSRV-CREX parametrization has been obtained by incorporating the recently measured neutron skin thickness $\Delta r_{np} = 0.121 \pm 0.026$ fm for ^{48}Ca using the parity-violating electron scattering experiment [21]. The parameters of BSRV-PREX model have been searched by incorporating the recently measured neutron skin thickness $\Delta r_{np} = 0.283 \pm 0.071$ fm for ^{208}Pb from the PREX-II data [21] in our fit. The BSRV-CPREX parametrizations has been obtained by incorporating both the CREX and PREX-II data for neutron skin thicknesses for ^{48}Ca and ^{208}Pb nuclei in the fit data. In addition, we have also included the maximum mass of neutron star [44] in our fit data.

TABLE I. Newly generated parameter sets BSRV-CREX, BSRV-PREX, and BSRV-CPREX for the Lagrangian of RMF model as given in Eq. (1) along with theoretical uncertainties/errors. The parameter $\overline{\kappa}$ is in fm^{-1}. The mass for nucleon, ω, ρ, and δ mesons are taken as $M_N = 939$ MeV, $m_\omega = 782.5$ MeV, $m_\rho = 762.468$ MeV, and $m_\delta = 980$ MeV, respectively. The values of $\overline{\kappa}$, $\overline{\lambda}$, and $\Lambda_{\omega\rho}$ are multiplied by 10^2. Parameters for NL3 [41], FSUGarnet [34], IOPB-1 [42], and Big Apple [43] are also shown for comparison.

Parameters	BSRV-CREX	BSRV-PREX	BSRV-CPREX	NL3	FSUGarnet	IOPB-1	Big Apple
g_σ	10.71506 ± 0.02086	10.40613 ± 0.08977	10.44537 ± 0.02480	10.21743	10.50315	10.41851	9.67810
g_ω	13.82692 ± 0.03539	13.37605 ± 0.13078	13.43408 ± 0.03477	12.86762	13.69695	13.38412	12.33541
g_ρ	16.18406 ± 1.20866	10.27951 ± 2.23787	10.28003 ± 2.15232	8.94880	13.87880	11.11560	14.14256
g_δ	4.27816 ± 0.75631	1.19517 ± 4.29242	1.70339 ± 3.97826	—	—	—	—
$\overline{\kappa}$	1.41726 ± 0.04886	1.64259 ± 0.04079	1.66238 ± 0.05821	1.95734	1.65229	1.85581	2.61776
$\overline{\lambda}$	0.46733 ± 0.08773	-0.08316 ± 0.09341	-0.20868 ± 0.19224	-1.59137	-0.035330	-0.075516	-2.16586
ζ	0.03441 ± 0.00130	0.02611 ± 0.00212	0.02429 ± 0.00326	0.00000	0.23486	0.017442	0.000699
$\Lambda_{\omega\rho}$	5.18286 ± 1.21735	2.90293 ± 2.60556	2.25722 ± 1.70126	0.00000	8.6000	4.80000	9.40000
m_σ	504.679 ± 0.689	502.050 ± 1.099	501.933 ± 1.600	508.194	496.731	500.487	492.975

For the open shell nuclei, the pairing has been included using BCS formalism with constant pairing gaps [45,46] that are taken from the nucleon separation energies of neighboring nuclei [39]. Neutron and proton pairing gaps are calculated by using the fourth-order finite difference mass formula (five-point difference) [47]. The neutron and proton pairing gaps (Δ_n, Δ_p) in MeV for the open shell nuclei are ^{68}Ni(1.46,0.0), ^{88}Sr(0.0,1.284), ^{90}Zr(0.0,1.239), ^{116}Sn(1.189,0.0), and ^{144}Sm(0.0,1.0). The neutron pairing gap for ^{24}O practically vanishes since the first unoccupied orbit $1d_{3/2}$ is almost 4.5 MeV above the completely filled $2s_{1/2}$ orbit [34,48]. The pairing correlation energies for a fix gap Δ is calculated by using the pairing window of $2\hbar\omega$, where $\hbar\omega = 45A^{-1/3}$–$25A^{-2/3}$ MeV [7,29]. We have obtained three different parametrizations by calibrating the parameters to a suitable set of finite nuclei as discussed earlier. Three different parametrizations obtained in the present work give an equally good fit to the properties of finite nuclei which were used for the optimization procedure. In Table I, We display the model parameters for the newly generated parameter sets BSRV-CREX, BSRV-PREX, and BSRV-CPREX along with theoretical uncertainties/errors. We also list the value of parameters for NL3 [41], FSUGarnet [34], IOPB-1 [42], and Big Apple [43] for comparison. It can be seen from the table that comparatively a large value of isovector scalar meson coupling parameter g_δ (4.27816), isovector vector meson coupling g_ρ (16.18406), and cross-coupling between ω and ρ meson quantified by the term $\Lambda_{\omega\rho}$ (5.18286) are obtained for BSRV-CREX parametrization in which only CREX data is included in the fit. The values of coupling parameters g_δ, g_ρ, and $\Lambda_{\omega\rho}$ is more or less the same for BSRV-PREX and BSRV-CPREX models. In Figs. 1–3 we show the color-coded plots for the correlation coefficients between the coupling parameters appearing in Lagrangian [Eq. (1)] for BSRV-CREX, BSRV-PREX, and BSRV-CPREX models. A strong correlation exists between the pairs of coupling parameters g_σ–g_ω, $\Lambda_{\omega\rho} - g_\delta$, and $\overline{\kappa} - \overline{\lambda}$ for BSRV-CREX model. The strong correlation is also observed for pair of coupling parameters g_σ–g_ω, g_ρ with g_δ and $\Lambda_{\omega\rho}$. For BSRV-CPREX model, a strong correlation is observed for g_δ with g_ρ, $\overline{\lambda}$ and ζ. The coupling parameter ζ is found to be well correlated with g_ρ and $\overline{\lambda}$. A strong correlation between the model parameters

indicates a strong interdependence, i.e., if one parameter is fixed at a certain value, then the other must attain the precise value as suggested by their correlation. It can be seen from Fig. 3 that when the skin thickness for ^{48}Ca and ^{208}Pb fitted together there is an overall reduction among the model parameters correlations as compared to those obtained by fitting the individual neutron skin.

B. Finite nuclei and infinite nuclear matter

In Table II, different observables fitted in the present work, their experimental values [39,40], adopted errors σ on them along with their calculated values for different BSRV parametrizations and theoretical uncertainties are displayed. The newly generated parametrizations BSRV-CREX, BSRV-PREX, and BSRV-CPREX give an
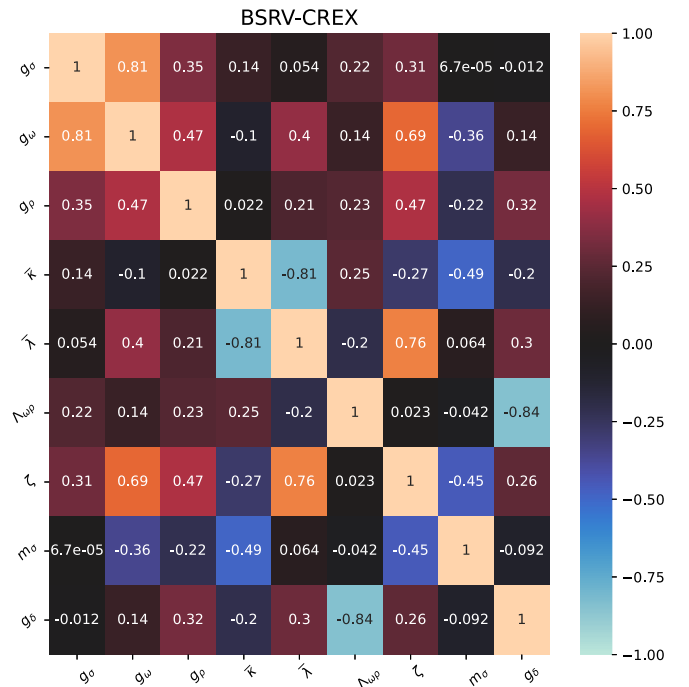

FIG. 1. Correlation coefficients among the model parameters of the Lagrangian given by Eq. (1) for BSRV-CREX parametrization.

TABLE II. The calculated values of binding energy (BE) and charge radii (r_{ch}) along with theoretical uncertainties/errors for various BSRV parametrizations are presented. The predicted value of neutron skin thickness $\Delta r_{np} = r_n - r_p$ is also depicted for various models. The corresponding experimental values of BE and r_{ch} [39,40] and Δr_{np} [21,22,49,50] are also listed. The adopted errors on the observables (σ) used for the optimization of parameters and the asymmetry parameter $\delta = (N - Z)/A$ for the nuclei are also displayed. The values of BE are given in units of MeV and r_{ch}, Δr_{np} are in fm.

Nucleus	Observables	Exp.	σ	δ	BSRV-CREX	BSRV-PREX	BSRV-CPREX	NL3	IOPB-I
^{16}O	BE	127.62	4.0	0.0	129.82 ± 0.32	128.71 ± 0.55	128.57 ± 0.60	127.08	128.05
	r_{ch}	2.699	0.04		2.690 ± 0.024	2.706 ± 0.031	2.709 ± 0.029	2.727	2.719
	Δr_{np}	—	—		-0.029 ± 0.020	-0.028 ± 0.009	-0.028 ± 0.008	-0.027	-0.029
^{24}O	BE	168.96	2.0	0.33	166.89 ± 1.41	170.71 ± 1.29	171.03 ± 1.15	170.54	169.48
	r_{ch}	—	—		2.753 ± 0.033	2.734 ± 0.011	2.732 ± 0.015	2.737	2.741
	Δr_{np}	—	—		0.559 ± 0.023	0.511 ± 0.010	0.632 ± 0.021	0.635	0.613
^{40}Ca	BE	342.04	3.0	0.0	344.53 ± 0.47	343.75 ± 0.56	343.51 ± 0.81	341.32	342.68
	r_{ch}	3.478	0.04		3.445 ± 0.035	3.455 ± 0.029	3.457 ± 0.014	3.469	3.464
	Δr_{np}	$-0.08^{+0.05}_{-1.0}$	—		-0.052 ± 0.002	-0.050 ± 0.012	-0.050 ± 0.002	-0.048	-0.050
^{48}Ca	BE	415.97	1.0	0.167	416.07 ± 0.46	415.46 ± 0.56	415.52 ± 0.60	414.52	414.57
	r_{ch}	3.477	0.04		3.475 ± 0.014	3.467 ± 0.010	3.467 ± 0.020	3.471	3.471
	Δr_{np}	0.121 ± 0.026	0.026		0.146 ± 0.019	0.212 ± 0.022	0.215 ± 0.018	0.226	0.199
^{56}Ni	BE	484.01	5.0	0.0	483.92 ± 0.62	481.55 ± 1.00	482.14 ± 0.78	482.12	482.48
	r_{ch}	3.750	0.02		3.709 ± 0.015	3.721 ± 0.015	3.718 ± 0.016	3.716	3.707
	Δr_{np}	$-0.03^{+0.08}_{-0.11}$	—		-0.038 ± 0.001	-0.037 ± 0.004	-0.036 ± 0.009	-0.034	-0.037
^{68}Ni	BE	590.41	2.0	0.176	592.43 ± 0.50	592.43 ± 0.53	592.35 ± 0.49	591.21	591.66
	r_{ch}	—	—		3.883 ± 0.015	3.866 ± 0.027	3.864 ± 0.020	3.863	3.869
	Δr_{np}	—	—		0.239 ± 0.019	0.310 ± 0.027	0.317 ± 0.029	0.333	0.299
^{78}Ni	BE	642.564	3.0	0.282	640.19 ± 1.24	641.61 ± 1.41	641.83 ± 1.27	643.04	640.55
	r_{ch}	—	—		3.971 ± 0.024	3.952 ± 0.015	3.950 ± 0.017	3.942	3.950
	Δr_{np}	—	—		0.403 ± 0.033	0.526 ± 0.123	0.535 ± 0.034	0.553	0.506
^{88}Sr	BE	768.42	2.0	0.136	768.51 ± 0.51	767.69 ± 0.55	767.62 ± 0.56	767.31	766.65
	r_{ch}		0.02		4.237 ± 0.013	4.227 ± 0.012	4.226 ± 0.014	4.225	4.229
	Δr_{np}	—	—		0.069 ± 0.009	0.130 ± 0.026	0.134 ± 0.021	0.148	0.118
^{90}Zr	BE	783.81	1.0	0.111	783.92 ± 0.59	783.19 ± 0.60	783.16 ± 0.62	782.95	782.44
	r_{ch}	4.269	0.02		4.289 ± 0.018	4.282 ± 0.012	4.282 ± 0.014	4.280	4.284
	Δr_{np}	$0.09^{+0.02}_{-0.02}$	-		0.033 ± 0.013	0.083 ± 0.022	0.086 ± 0.018	0.097	0.072
^{100}Sn	BE	825.10	2.0	0.0	827.55 ± 0.97	826.96 ± 1.04	827.55 ± 1.34	829.33	827.52
	r_{ch}	—	—		4.515 ± 0.014	4.522 ± 0.014	4.521 ± 0.026	4.511	4.514
	Δr_{np}	—	—		-0.129 ± 0.002	-0.126 ± 0.018	-0.125 ± 0.002	-0.117	-0.126
^{116}Sn	BE	988.67	2.0	0.138	987.42 ± 0.65	987.15 ± 0.72	986.85 ± 0.69	986.89	986.24
	r_{ch}	4.627	0.02		4.631 ± 0.017	4.617 ± 0.015	4.617 ± 0.014	4.610	4.620
	Δr_{np}	$0.10^{+0.03}_{-0.03}$	-		0.098 ± 0.013	0.163 ± 0.024	0.169 ± 0.028	0.183	0.149
^{132}Sn	BE	1102.22	2.0	0.242	1102.55 ± 0.94	1102.51 ± 1.05	1102.37 ± 0.96	1104.81	1101.93
	r_{ch}	4.709	0.02		4.742 ± 0.013	4.723 ± 0.019	4.722 ± 0.014	4.710	4.721
	Δr_{np}	-	-		0.226 ± 0.025	0.348 ± 0.048	0.357 ± 0.025	0.383	0.325
^{144}Sm	BE	1195.77	2.0	0.139	1197.69 ± 0.82	1197.21 ± 0.91	1196.90 ± 0.82	1198.14	1195.82
	r_{ch}	—	—		4.978 ± 0.021	4.965 ± 0.102	4.965 ± 0.014	4.956	4.967
	Δr_{np}	-	-		0.047 ± 0.013	0.116 ± 0.023	0.121 ± 0.031	0.137	0.103
^{208}Pb	BE	1636.34	1.0	0.212	1637.11 ± 0.92	1636.57 ± 0.94	1636.00 ± 0.93	1639.43	1636.75
	r_{ch}	5.501	0.04		5.551 ± 0.016	5.533 ± 0.018	5.532 ± 0.029	5.517	5.532
	Δr_{np}	0.283 ± 0.071	0.071		0.130 ± 0.018	0.243 ± 0.048	0.252 ± 0.028	0.279	0.219
		(0.18 ± 0.07) [49]	-						

equally good fit to the properties of finite nuclei. The fitted values of finite nuclei are quite close to their experimental values. The root-mean square (rms) errors in total binding energy for all the nuclei considered in our fit are found to be 1.62, 1.39, and 1.39 MeV, whereas the rms errors in total charge radii are 0.071, 0.080, and 0.081 fm for BSRV-CREX, BSRV-PREX, and BSRV-CPREX parameter sets, respectively. We also depict the predicted values of neutron skin thickness $\Delta r_{np} = R_n - R_p$ and charge rms radii (r_{ch}) for all our parametrizations. It can be observed from the table that for BSRV-CREX parametrization, the value of Δr_{np} for ^{48}Ca nucleus is 0.146 ± 0.019 fm and is consistent with the recently reported value of Δr_{np} of ^{48}Ca from CREX data [21] while the value of Δr_{np} for ^{208}Pb nucleus comes out to be 0.13 ± 0.018 fm that is also in good agreement with the value reported for neuton skin thickness of $\Delta r_{np} = (0.18 \pm 0.07)$ fm for ^{208}Pb obtained by dispersive optical model analysis of the Washington University group [49]. The values of
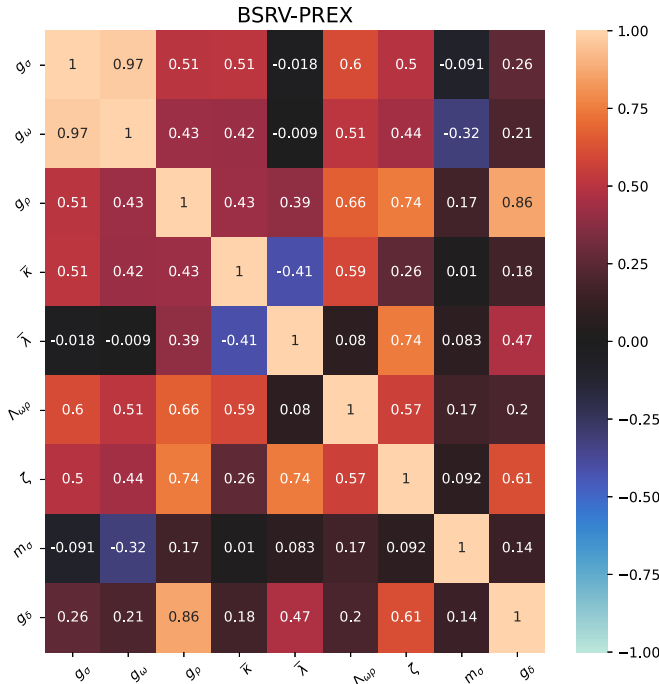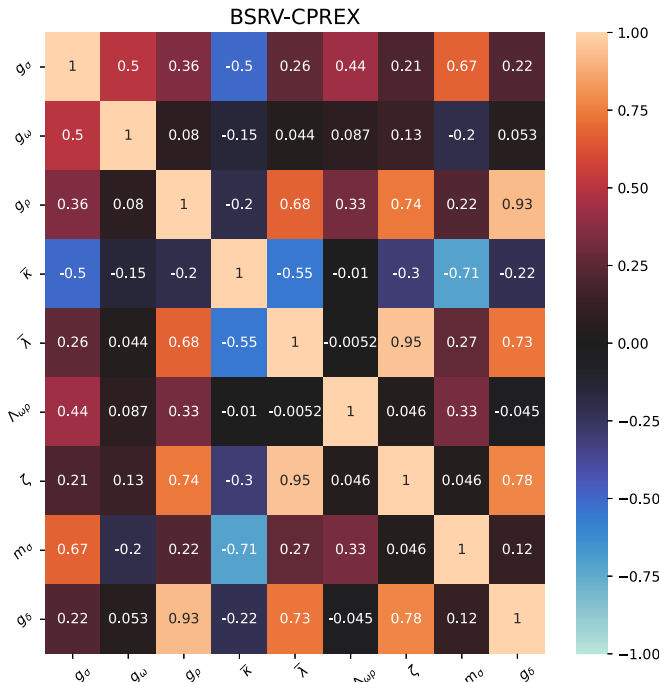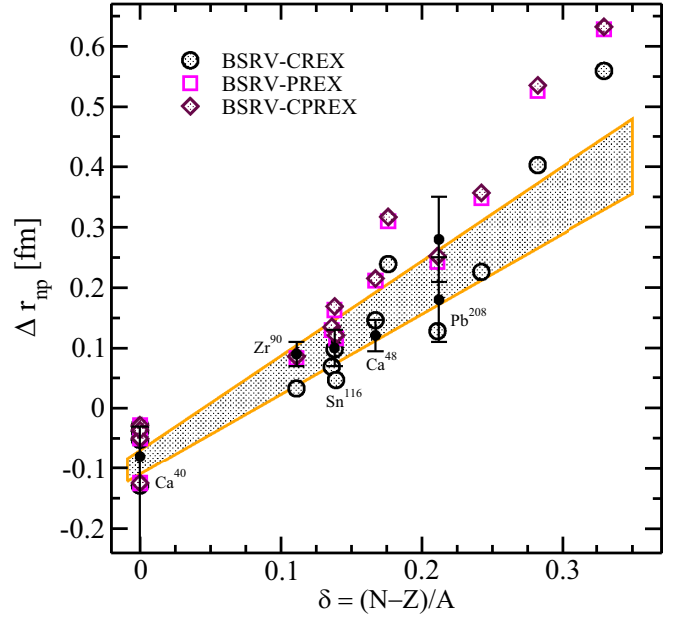
FIG. 2. Same as Fig. 1 but for BSRV-PREX parametrization.

FIG. 4. Variation of neutron skin thickness predicted for the nuclei considered in the fit data as a function of asymmetry parameter (δ). The shaded region is calculated by using Eq. (19).

Δr_{np} obtained for ^{208}Pb using the BSRV-CREX model does not satisfy the PREX-II measurement. The values of Δr_{np} for ^{208}Pb obtained for BSRV-PREX and BSRV-CPREX parametrizations is in good agreement with the recently reported value $\Delta r_{np} = (0.283 \pm 0.071)$ fm for ^{208}Pb for PREX-II data, but the value of Δr_{np} predicted for ^{48}Ca overestimates the CREX data [21]. In Fig. 4 we show the neutron skin thickness Δr_{np} for nuclei considered in our

data fit as a function of neutron-proton asymmetry parameter $\delta = \frac{N-Z}{A}$. The predicted result of Δr_{np} for the nuclei used in our fit data (Table II) for BSRV-CREX, BSRV-PREX, and BSRV-CPREX parametrizations are compared with the corresponding available experimental values along with error bars taken from Refs. [21,22,49,50]. The shaded regions represent the linear dependence of neutron skin thickness on asymmetry (neutron excess) δ of a nucleus that can be fitted by [50,51]

$$\Delta r_{np} = (-0.09 \pm 0.02) + (1.45 \pm 0.12)\delta \quad \text{(fm)}. \quad (19)$$

The values of Δr_{np} obtained for BSRV-PREX and BSRV-CPREX parameter sets for some of the nuclei deviate from shaded region as can be observed from Fig. 4. This may be attributed to the fact that for these paramerizations the value of ω-ρ meson coupling parameter $\Lambda_{\omega\rho}$ that constrains the density dependence of symmetry energy and coupling parameters g_{δ} and g_{ρ} is relatively smaller as compared to BSRV-CREX parameter set. For BSRV-CREX parameter set, the values of Δr_{np} lie in the shaded region or very close to it except for ^{24}O nucleus for which asymmetry is 0.33. For BSRV-CREX, BSRV-PREX, and BSRV-CPREX models, the calculated values of neutron skin thickness for ^{208}Pb nucleus are 0.130 ± 0.018 fm, 0.243 ± 0.048 fm, and 0.252 ± 0.028 fm and for ^{48}Ca nucleus are 0.146 ± 0.019 fm, 0.212 ± 0.022 fm, and 0.215 ± 0.018 fm, respectively. The value of $\Delta r_{np} = 0.146 \pm 0.019$ fm for ^{48}Ca predicted by BSRV-CREX is consistent with the recently measured $\Delta r_{np} = 0.121 \pm 0.026$ fm from parity-violating electron scattering experiment (CREX) [21]. The values of neutron skin thickness $\Delta r_{np} = 0.243 \pm 0.048$ fm and 0.252 ± 0.028 fm predicted for ^{208}Pb by BSRV-PREX and BSRV-CPREX are also in agreement with the recently reported neutron skin thickness from updated PREX-II [22].

FIG. 3. Same as Fig. 1 but for for BSRV-CPREX parametrization.

TABLE III. The bulk nuclear matter properties at saturation density along with theoretical uncertainties for BSRV-CREX, BSRV-PREX and BSRV-CPREX parametrizations are listed along with NL3, IOPB-1, FSUGarnet and Big Apple models. ρ_0, E/A, K, J, L, K_{sym}, and M^*/M denotes the saturation density, binding energy per nucleon, incompressibility coefficient, symmetry energy, density dependence of symmetry energy, the curvature of symmetry energy, and the ratio of effective nucleon mass to the nucleon mass, respectively.

Parameters	BSRV-CREX	BSRV-PREX	BSRV-CPREX	NL3	IOPB-1	FSUGarnet	Big Apple
ρ_0 (fm^{-3})	0.148 ± 0.003	0.148 ± 0.001	0.148 ± 0.002	0.148	0.149	0.153	0.155
E/A (MeV)	-15.99 ± 0.03	-16.10 ± 0.06	-16.09 ± 0.05	-16.24	-16.09	-16.23	-16.34
K (MeV)	222.29 ± 13.08	227.45 ± 6.95	226.99 ± 3.74	271.56	222.57	229.62	227.09
M^*/M	0.600 ± 0.007	0.606 ± 0.004	0.602 ± 0.006	0.595	0.593	0.578	0.608
J (MeV)	28.97 ± 0.99	34.41 ± 2.71	34.99 ± 2.15	37.40	33.30	30.98	31.41
L (MeV)	30.61 ± 6.74	77.08 ± 28.87	82.32 ± 22.93	118.56	63.85	50.92	40.33
K_{sym}(MeV)	61.79 ± 32.74	-71.48 ± 5.53	-65.65 ± 20.32	100.90	-37.79	58.46	89.58

In the present work, we have tried to resolve the serious conflict of CREX and PREX-II measurements by searching the model parameters of BSRV-CPREX parametrization by including both the Δr_{np} of ^{48}Ca from the CREX and ^{208}Pb from PREX-II in our fit data for the optimization of model parameters. But the Δr_{np} predicted by this model overestimates the recently reported value by CREX and the serious conflict between CREX and PREX-II measurements continues as also discussed in Ref. [52].

In Table III, we present our results for the symmetric nuclear matter (SNM) properties such as binding energy per nucleon (E/A), incompressibility (K), symmetry energy coefficient (J), density dependence of symmetry energy (L), and ratio of effective mass to the mass of nucleon at the saturation density (ρ_0) and curvature of symmetry energy (K_{sym}) along with theoretical uncertainties. These properties play a vital role for constructing the EoS for nuclear matter. E/A is more or less the same for all BSRV's parametrizations. For newly generated parametrizations BSRV-PREX and BSRV-CPREX, the values of J and L are consistent with the constraints from observational analysis $J = 38.1 \pm 4.7$ MeV and $L = 106 \pm 37$ MeV as reported by Reed *et al.* [26] and for BSRV-CREX parameter set, the values of $J = 28.97 \pm 0.99$ MeV and $L = 30.61 \pm 6.74$ MeV are in close proximity to that reported in Ref. [52], it is also consistent with the constraints from observational analysis $J = 31.6 \pm 2.66$ MeV [53]. The neutron skin thickness as reported by CREX collaboration suggests softness, i.e., low value of symmetry energy coefficient (J) and its corresponding density dependence (L). The value of K lies in the range 222.29 ± 13.08–227.45 ± 6.95 MeV which is also in good agreement with the value of $K = 240 \pm 20$ MeV determined from isoscalar giant monopole resonance (ISGMR) for ^{90}Zr and ^{208}Pb nuclei [54,55]. The curvature of symmetry energy K_{sym} also satisfies the empirical limit discussed in [56]. The ratio of effective mass to the nucleon mass is found to be similar for all BSRV's parametrizations as shown in Table III. The SNM properties calculated with NL3, FSUGarnet, IOPB-1, and Big Apple are also shown for comparison.

In Figs. 5 and 6, we plot the EoS, i.e., pressure as a function of baryon density scaled to saturation density ($\frac{\rho}{\rho_0}$) for SNM and pure neutron matter (PNM) using BSRV-CREX, BSRV-PREX and BSRV-CPREX parametrizations which are in good agreement and lie in the allowed region with the

EoS extracted from the analysis of particle flow in heavy ion collision [28]. These results are also compared with the NL3, IOPB-1, FSUGarnet, and Big Apple parametrizations. It can be easily seen that the EoSs for SNM and PNM obtained from NL3 and Big Apple parametrizations are very stiff and are ruled out by constraints imposed by heavy ion collision data. The stiffness of the EoSs for NL3 and Big Apple parameter sets may be due to the fact that the coupling parameter ζ which is responsible for varying the high-density behavior of EoS is zero for NL3 and very small for Big Apple parameter sets. The EoSs calculated using BSRV's parameter sets are relatively much softer and lie in the allowed region of heavy ion collision data [28]. The EoS calculated from BSRV-CREX parametrization is the softest amongst all EoSs and it might be due to the relatively somewhat higher value of parameter ζ and $\Lambda_{\omega\rho}$ obtained for this parameter set during
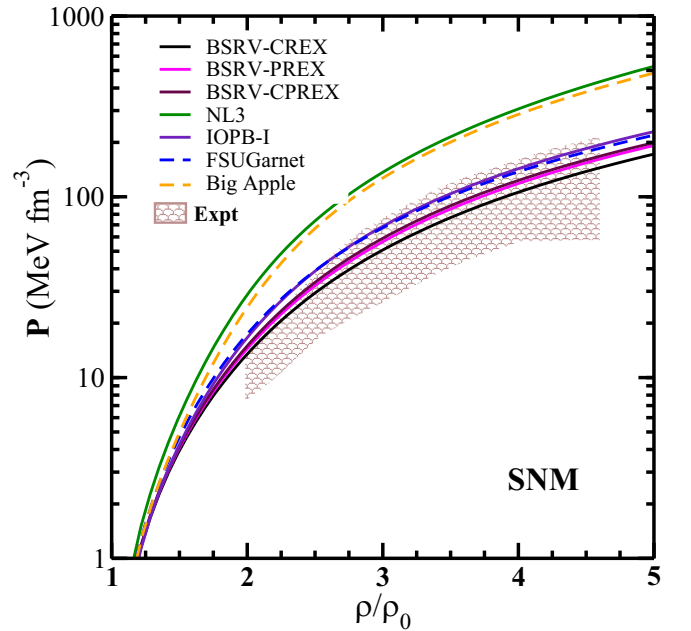

FIG. 5. Variation of Pressure as a function of baryon density for symmetric nuclear matter (SNM) computed with BSRV's parametrizations along with NL3, IOPB-1, FSUGarnet, and Big Apple models. The shaded region represents the experimental data taken from the reference [28].
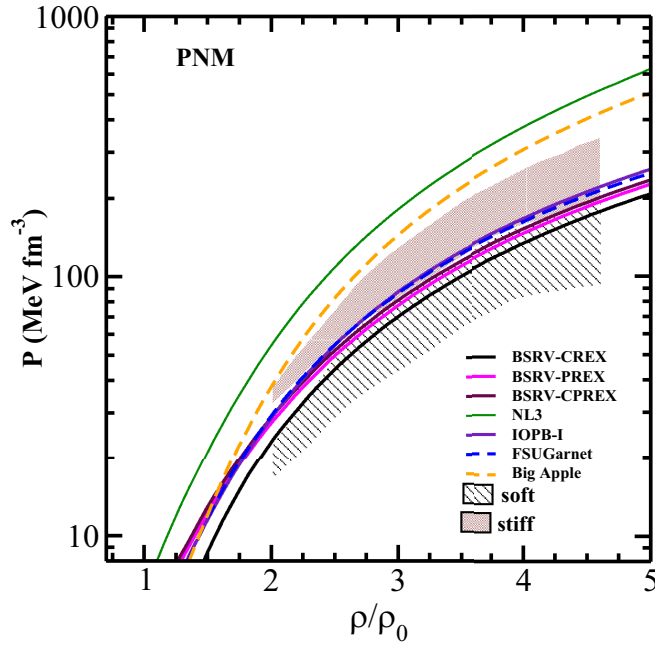
FIG. 6. Variation of Pressure as a function of baryon density for pure neutron matter (PNM) computed with BSRV's parametrizations along with NL3, IOPB-1, FSUGarnet, and Big Apple models. The shaded region represents the experimental data taken from the reference [28].

the calibration procedure which is responsible for varying high-density behavior of EoS. In Fig. 7 we plot the density dependence of symmetry energy (L) as a function of baryon density for BSRV's paramerizations. The results for NL3,
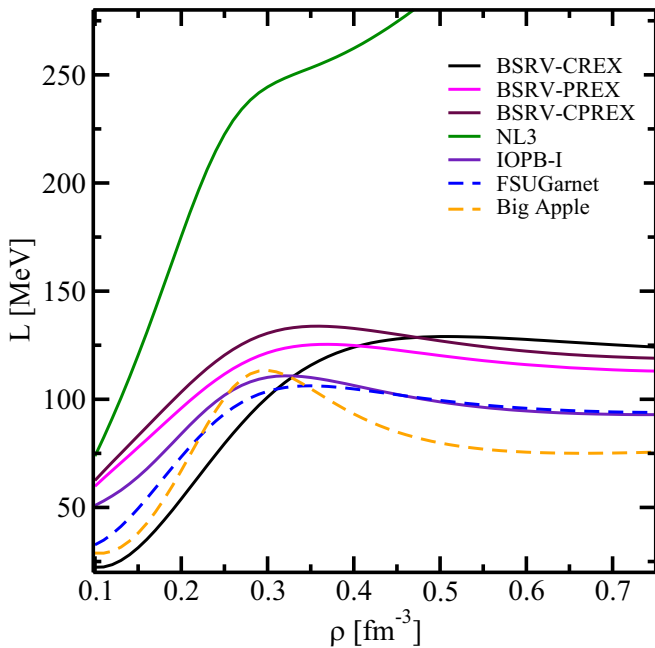

FIG. 7. Variation of density dependence of symmetry energy (L) as a function of baryon density for various parametrizations considered in the present work.
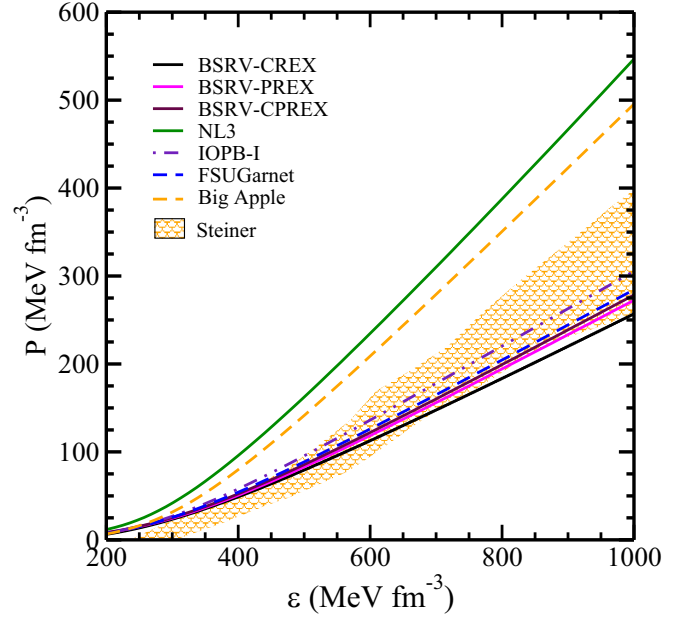
FIG. 8. EoSs, i.e., pressure as a function of energy density for β-stable equilibrated nuclear matter for various parametrizations. The shaded region represents the observational constraints reported in Ref. [57].

IOPB-1, FSUGarnet, and Big Apple parameter sets are also displayed for comparison. It can be seen from the figure that in low or medium density regime the behvior of BSRV-CREX is softest (low value of L at a given baryon density) among all parametrizations and changes to stiffest in high density regime even though the Δr_{np} for ^{208}Pb nucleus is smallest for this parameter set. This may be attributed to the large value of coupling parameter g_δ (4.27816) obtained for BSRV-CREX parameter set. The coupling parameter g_δ is responsible for changing the behivior of L from soft in low-medium density regime to stiff in high density regime. The stiffness of L for BSRV-PREX and BSRV-CPREX parameter sets may also be due to the coupling parameter g_δ and large value of Δr_{np} for ^{208}Pb nucleus. A large value of Δr_{np} for ^{208}Pb in case of NL3 parameter and its small value for Big Apple may be responsible for for stiffness and softness behavior of L, respectively.

C. Neutron star properties

In Fig. 8 we display the EoS, i.e., the variation of pressure with the energy density for the neutron star in β equilibrium for all BSRV's parametrizations. The results calculated with NL3, IOPB-1, FSUGarnet, and Big Apple parameter sets are also shown for comparison. The shaded region in Fig. 8 represents the observational constraints at $r_{\rm ph} = R$ with the uncertainty of 2σ [57]. Here $r_{\rm ph}$ and R are the photospheric and neutron star radius, respectively. It can be observed from the figure that the EoS computed with newly generated BSRV's parameter sets are softer and lie in the lower boundary of the shaded region at very high density ($\mathcal{E} \approx 700$–1000 MeV fm^{-3}). The softness of EoSs for BSRV's parameter sets may be due to the moderate value of ω meson coupling
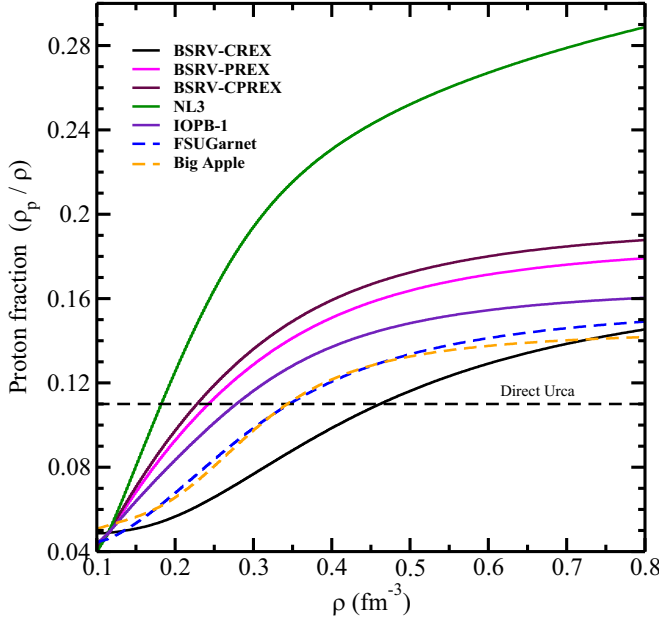
FIG. 9. The plot of proton fractions as a function of baryon density. The dotted horizontal line represents the threshold for the direct Urca process, i.e., $(\rho_p/\rho) = 0.11$ [58].
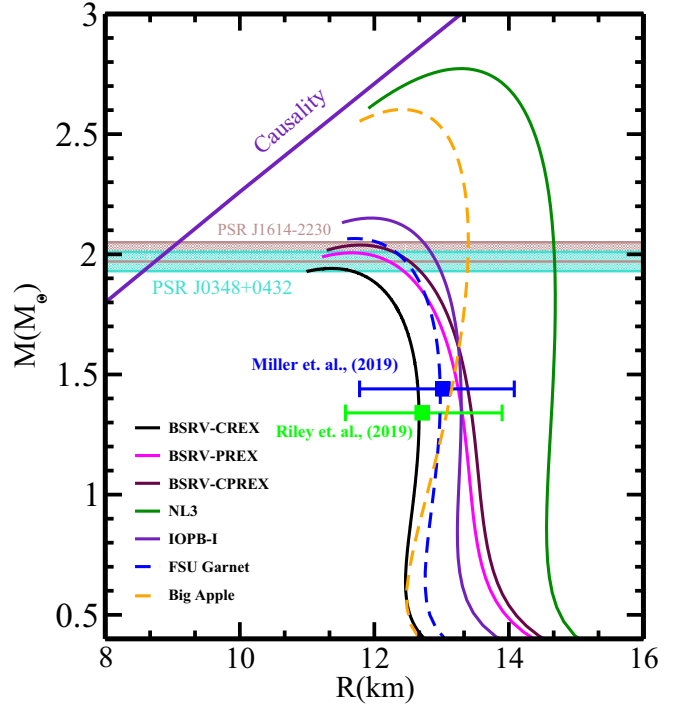

FIG. 10. Variation of the gravitational mass of nonrotating neutron stars as a function of radius. for BSRV's parametrizations. The results for NL3, IOPB-1, FSUGarnet, and Big Apple parameter sets are also shown.

parameter ζ that governs the high-density behavior of EoS. The EoSs calculated for NL3 and Big Apple parameter sets are stiffer and may be attributed to either zero or very small value of coupling parameter ζ for these parameter sets, respectively. In Fig. 9 we illustrate the proton fraction in neutron star matter. One remarkable point is that the g_δ has an influence on proton fraction at high densities. The large value of g_δ for BSRV-CREX suppresses the proton fraction and then delays the direct Urca process in which neutrinos can be emitted rapidly. It can also be observed that Δr_{np} of ^{208}Pb nucleus also plays a significant role in the direct Urca process. The large value of Δr_{np} for ^{208}Pb may be attributed to the early start of the direct Urca process for BSRV-PREX, BSRV-CPREX, and NL3, whereas its small value for BSRV-CREX parameter set may be responsible for delayed direct Urca process for BSRV-CREX parametrization.

The mass and radius of a neutron star are obtained by solving the Tolman-Oppenheimer-Volkoff (TOV) equations [59,60] given as

$$\frac{dP(r)}{dr} = -\frac{\{\epsilon(r) + P(r)\}\{4\pi r^3 P(r) + m(r)\}}{r^2[1 - 2m(r)/r]}, \quad (20)$$

$$\frac{dm}{dr} = 4\pi r^2 \epsilon(r), \quad (21)$$

$$m(r) = 4\pi \int_0^r dr\, r^2 \epsilon(r), \quad (22)$$

where $P(r)$ is the pressure at radial distance r and $m(r)$ is the mass of neutron stars enclosed in the sphere of radius r. In Fig. 10 we plot the results for the gravitational mass of a nonrotating neutron star and its radius for BSRV-CREX, BSRV-PREX, and BSRV-CPREX parameter sets. The results are also displayed for NL3, IOPB-1, FSUGarnet, and

Big Apple parametrizations. It is observed that the maximum gravitational mass of the nonrotating neutron star for BSRV's parameter sets lies in the range $1.95 \pm 0.04 M_\odot$– 2.04 ± 0.04 $M_\odot$ which is in good agreement with the mass constraints from GW170817 event, pulsars PSRJ1614-2230, PSRJ0348+0432, and PSRJ0740+6620 [13,44,61–63]. The EoS for β-equilibrated matter calculated with BSRV-CREX model is the softest amongst all parametrizations considered in this work. The radius of canonical mass ($R_{1.4}$) including BPS crust [64] for low-density region is 12.66 ± 0.39 Km, 13.27 ± 0.55 Km and 13.41 ± 0.71 Km for BSRV-CREX, BSRV-PREX, and BSRV-CPREX parametrizations which satisfies the radius constraints from NICER on $R_{1.4}$ and PREX-II reported in Ref. [26]. The value of $R_{1.4}$ for BSRV's paramerization is consistent with the softness and stiffness behavior of symmetry energy coefficient. The value of $R_{1.4}$ for NL3 parametrization is 14.65 Km which seems to be ruled out by the constraints for $R_{1.4}$ extracted from Ref. [65].

The tidal deformability rendered by the companion stars on each other in a binary system can provide significant information on the EoS of neutron stars [66,67]. The tidal influences of its companion in the binary neutron star (BNS) system will deform neutron stars in the binary system and, the resulting change in the gravitational potential modifies the BNS orbital motion and its corresponding gravitational wave (GW) signal. This effect on GW phasing can be parameterized by the dimensionless tidal deformability parameter, $\Lambda_i = \lambda_i/M_i^5$, $i = 1, 2$. For each neutron star, its quadrupole moment $\mathcal{Q}_{j,k}$ must be related to the tidal field $\mathcal{E}_{j,k}$ caused
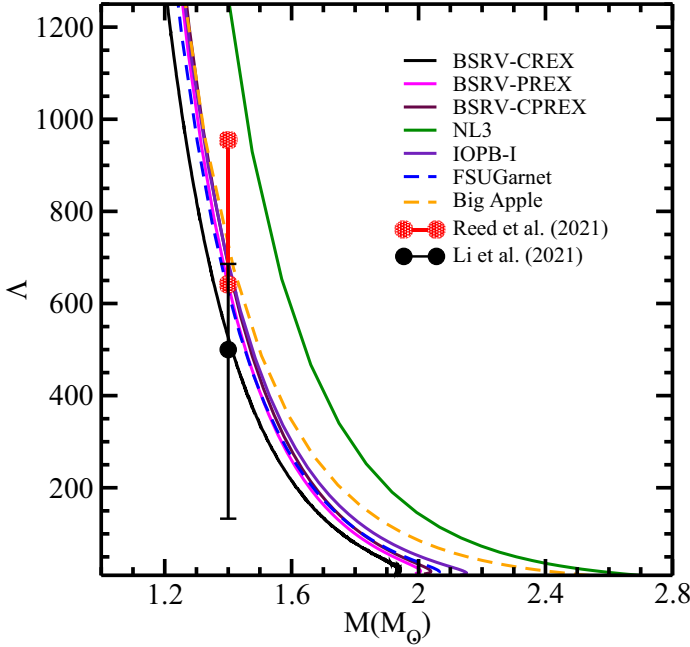
FIG. 11. Variation of dimensionless tidal deformability (Λ) with respect to gravitational mass for all BSRV's parametrizations. The results for NL3, IOPB-1, FSUGarnet, and Big Apple parameter sets are also shown.
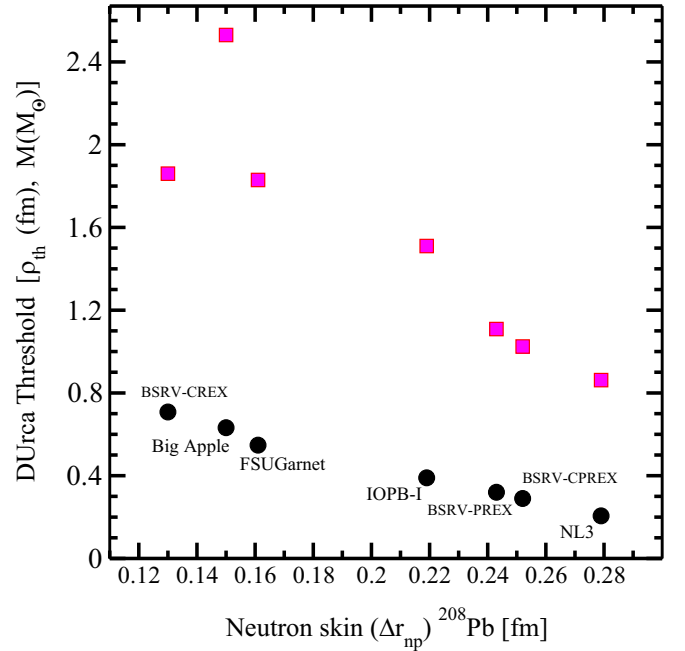

FIG. 12. The thresholds for the onset of direct Urca Process in neutron stars. The threshold density is represented by the solid black circles and the corresponding neutron star mass for such central density is depicted by solid magenta squares.

by its companion as, $\mathcal{Q}_{j,k} = -\lambda \mathcal{E}_{j,k}$, where j and k are spatial tensor indices. The dimensionless tidal deformability parameter Λ of a static, spherically symmetric compact star depends on the neutron star compactness parameter C and a dimensionless quadrupole Love number k_2 as $\Lambda = (2k_2/3)C^{-5}$. The Λ critically parameterizes the deformation of neutron stars under the given tidal field, therefore it should depend on the EoS of nuclear dense matter. To measure the Love number k_2 along with the evaluation of the TOV equations we have to compute $y_2 = y(R)$ with initial boundary condition $y(0) = 2$ from the first-order differential equation [66–69] simultaneously,

$$y' = \frac{1}{r}[-r^2Q - ye^\lambda\{1 + 4\pi Gr^2(P - \mathcal{E})\} - y^2], \quad (23)$$

where $Q \equiv 4\pi Ge^\lambda(5\mathcal{E} + 9P + \frac{\mathcal{E}+P}{c_s^2}) - 6\frac{e^\lambda}{r^2} - \nu'^2$ and $e^\lambda \equiv (1 - \frac{2Gm}{r})^{-1}$ and, $\nu' \equiv 2G e^\lambda (\frac{m+4\pi Pr^3}{r^2})$. First, we get the solutions of Eq. (23) with boundary condition, $y_2 = y(R)$, then the electric tidal Love number k_2 is calculated from the expression as

$$k_2 = \frac{8}{5}C^5(1-2C)^2[2C(y_2-1) - y_2 + 2]\Big\{2C(4(y_2+1)C^4$$
$$+ (6y_2 - 4)C^3 + (26 - 22y_2)C^2 + 3(5y_2 - 8)C$$
$$- 3y_2 + 6) - 3(1-2C)^2(2C(y_2-1) - y_2 + 2)$$
$$\times \log\left(\frac{1}{1-2C}\right)\Big\}^{-1}. \quad (24)$$

In Fig. 11, we display the results of dimensionless tidal deformability Λ as a function of gravitational mass for neutron stars for BSRV's parametrizations. For the sake of compari-

son, we also display the results calculated with NL3, IOPB-1, FSUGarnet, and Big Apple parametrizations. The values of $\Lambda_{1.4}$ obtained for canonical mass are 525.84 ± 151.48, 638.51 ± 142.03 and 682.57 ± 219.73 corresponding to BSRV-CREX, BSRV-PREX, and BSRV-CPREX, respectively, and satisfy the constraints as reported in Ref. [26,70,71]. It may be noted that the value of tidal deformability of $1.4M_\odot$ neutron star obtained for BSRV-PREX and BSRV-CPREX models have overlap with the revised limit of $\Lambda_{1.4} \leqslant 580$ within 1σ uncertainty [15]. The value (525.84 ± 151.48) of $\Lambda_{1.4}$ obtained for the BSRV-CREX parameter set is also consistent with the constraints imposed in Ref. [15]. This might be attributed to the high value of coupling g_δ for this parametrization that governs the softness and stiffness of EoS in the low and the high-density regime.

In Table IV, we summarize the results for nonrotating neutron star properties such as maximum gravitational mass (M), neutron star radius corresponding to the maximum mass ($R_{\max}$), radius $R_{1.4}$, radius $R_{2.0}$, and tidal deformability (Λ) corresponding to canonical and maximum mass of neutron star along with theoretical uncertainties. In Fig. 12 we plot the threshold central density (solid black circles) and corresponding neutron star mass (solid magenta squares) as a function of neutron skin thickness for the onset of the direct Urca process for BSRV's parameter sets. Similar results for NL3, IOPB-1, FSUGarnet, and Big Apple models are also displayed. It can be observed that the onset of the Urca process has a strong dependence on neutron skin thickness of ^{208}Pb and hence on symmetry energy coefficient. In particular, stiff symmetry energy as suggested by PREX-II favors large proton fractions that may trigger the onset of direct Urca process at

TABLE IV. The properties of nonrotating neutron stars for the various EoSs computed with BSRV parameter sets are displayed along with theoretical uncertainties on them. $M_{\max}(M_\odot)$ and $R_{\max}$ denote the maximum gravitational mass and radius corresponding to the maximum mass of the nonrotating neutron stars, respectively. The values for $R_{\max}$, $R_{1.4}$, and $\Lambda_{1.4}$ denote radius and dimensionless tidal deformability corresponding to $M_{\max}$ and $1.4M_\odot$.

SN	EoS	$M_{\mathbf{max}}(M_\odot)$	$R_{\mathbf{max}}$ (km)	$R_{\mathbf{1.4}}$ (km)	$\Lambda_{1.4}$
1.	BSRV-CREX	1.95 ± 0.04	11.34 ± 0.21	12.66 ± 0.39	525.84 ± 151.48
2	BSRV-PREX	2.01 ± 0.04	11.67 ± 0.26	13.27 ± 0.55	638.51 ± 142.03
3.	BSRV-CPREX	2.04 ± 0.04	11.79 ± 0.29	13.41 ± 0.71	682.57 ± 219.73
4.	NL3	2.77	13.28	14.65	1274
5	IOPB-I	2.15	11.95	13.29	682
6	FSUGarnet	2.06	11.65	12.98	622.51
7	Big Apple	2.60	12.41	13.12	715.96

lower central density [26]. It is evident from the figure that the onset of the direct Urca process is delayed with the decrease in the Δr_{np} of the ^{208}Pb. The threshold density for the onset of the direct Urca process for the BSRV-CREX model is 0.71 fm^{-3}. This high value is attributed to the small neutron skin thickness and soft L for BSRV-CREX. The threshold density for the onset of the direct Urca process decreases from 0.71 fm^{-3} to 0.21 fm^{-3} as the value of Δr_{np} for ^{208}Pb increases from 0.13 fm (BSRV-CREX) to 0.28 fm (NL3). The neutron star mass corresponding to threshold central density for the direct Urca process decreases from 2.53 to 0.86 $M_\odot$ for the parametrizations considered in the present work.

D. Correlations amongst nuclear matter observables and model parameters

In this subsection, we discuss the correlations between nuclear matter observables and model parameters. In Figs. 13–15, we display the correlations of bulk nuclear matter properties at saturation density and neutron star observables with the model parameters for BSRV's parametrizations.

For the BSRV-CREX model, the isoscalar bulk nuclear matter properties like K, M^*/M show strong correlations with isoscalar parameters $\overline{\kappa}$. It can also be observed from the Fig. 13 that the symmetry energy coefficients (J), its density dependence (L), and curvature of symmetry energy K_{sym} can be well constrained by the coupling parameter g_ρ as suggested by their correlations. The neutron star observables like $M_{\max}$, $R_{1.4}$, and $\Lambda_{1.4}$ display strong correlations with couplings $\Lambda_{\omega\rho}$ and g_δ. A strong correlation between $M_{\max}$ and ω-meson self-coupling parameter ζ is missing in the case of BSRV-CREX parametrization. The parameter g_δ might be responsible for the large maximum mass of neutron star as it makes the EOS somewhat stiffer at high density and thus weakens the correlation between $M_{\max}$ and ζ.

For the BSRV-PREX model, the isoscalar bulk nuclear matter properties like E/A, K, and M^*/M show strong correlations with isoscalar parameters g_σ and g_ω. As expected, a strong correlation of the isovector properties like J, L, and Δr_{np} for ^{208}Pb with isovector parameters g_ρ and $\Lambda_{\omega\rho}$ is observed. The neutron star observables like $M_{\max}$, $R_{1.4}$ and $\Lambda_{1.4}$ display good correlations with coupling g_δ and weak correlations with ζ. This suggests that the neutron star ob-

servables results from a competition between g_δ and ζ. For the BSRV-CPREX model, J, L, and Δr_{np} for ^{208}Pb are very well constrained by couplings g_ρ and $\Lambda_{\omega\rho}$ as can be observed from their correlations. K_{sym} shows strong dependence upon $\Lambda_{\omega\rho}$. The Δr_{np} for ^{48}Ca is very well constrained by g_ρ, g_δ, and $\Lambda_{\omega\rho}$. The $R_{1.4}$ and $\Lambda_{1.4}$ is found to have strong correlation with g_δ. These findings are quite in harmony with the results reported in Refs. [34,36].

V. SUMMARY

Three relativistic interactions BSRV-CREX, BSRV-PREX, and BSRV-CPREX for the relativistic mean-field model have been generated keeping in view the recently reported constraints on neutron skin thickness of ^{48}Ca (CREX) and ^{208}Pb nuclei by PREX-II data. The precise measurements of neutron skin thickness give an opportunity to modify or readjust
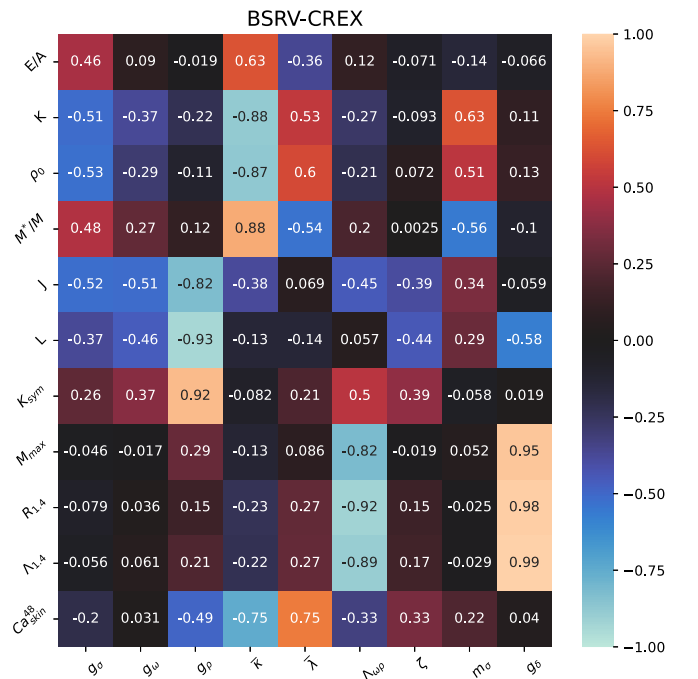

FIG. 13. Correlation coefficients amongst neutron star observables as well as the bulk properties of nuclear matter at the saturation density and model parameters for BSRV-CREX parametrization.
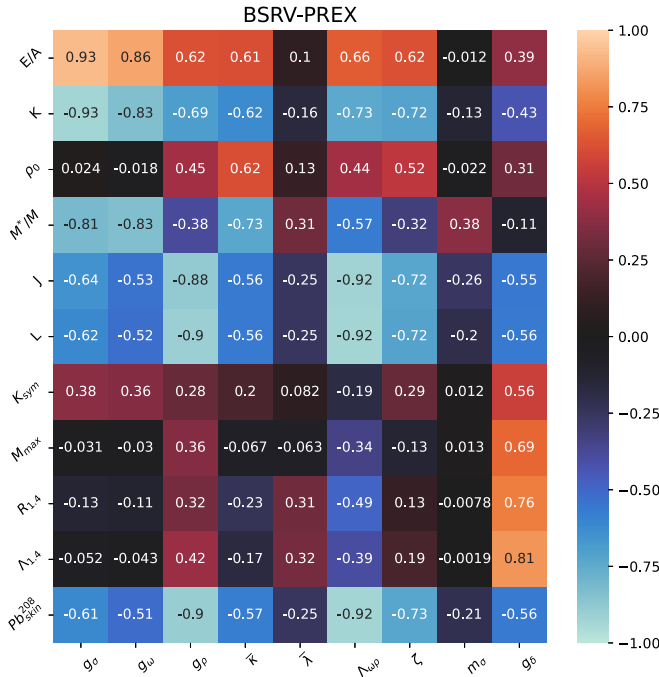
FIG. 14. Same as Fig. 13, but for BSRV-PREX paramerization.

the coupling constants of RMF models without compromising the bulk properties of nuclear matter and neutron stars. The Lagrangian density for the RMF model used in the present work is based on different nonlinear, self- and inter-couplings among isoscalar-scalar σ, isoscalar-vector ω_μ, isovector-scalar δ, and isovector-vector ρ_μ meson fields and nucleonic Dirac field Ψ. The BSRV-CREX parametrization has been obtained by incorporating the recently measured neutron skin thickness $\Delta r_{np} = 0.121 \pm 0.026$ fm for ^{48}Ca
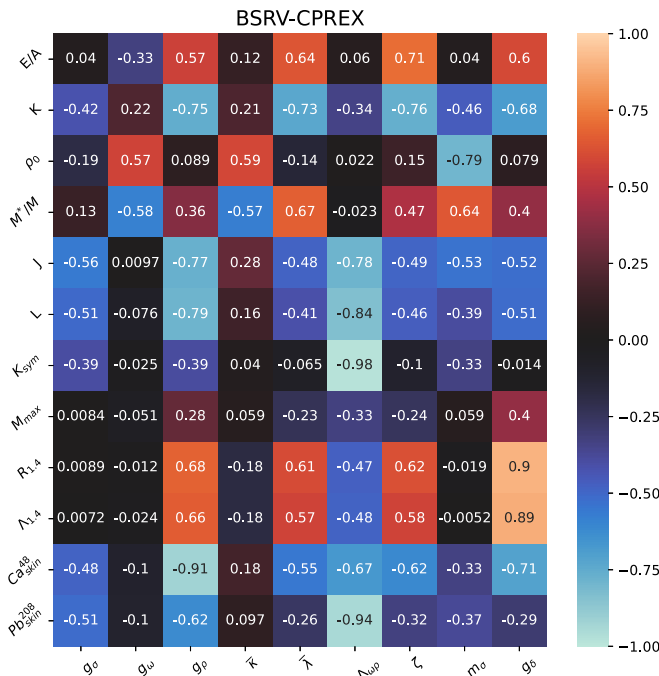

FIG. 15. Same as Fig. 13 but for BSRV-CPREX paramerization.

using the parity-violating electron scattering experiment [21]. The parameters of the BSRV-PREX model have been searched by incorporating the recently measured neutron skin thickness $\Delta r_{np} = 0.283 \pm 0.071$ fm for ^{208}Pb from the PREX-II [21] in our fit. The BSRV-CPREX parametrizations have been obtained by including both the CREX and PREX-II data for neutron skin thicknesses for ^{48}Ca and ^{208}Pb nuclei in the fitting data. The BSRV's parameter sets reproduce the ground state properties of the finite nuclei, bulk nuclear matter and also satisfy the constraints on mass and radius along with dimensionless deformability (Λ) of a neutron star from recent astrophysical observations [15,26,57,65]. All the BSRV's parametrizations give an equally good fit to the finite nuclear properties. The Bulk nuclear matter properties obtained are well consistent with the current empirical data [26,52,55]. The maximum gravitational mass and radius ($R_{1.4}$) of the neutron star lie in the range between 1.95 ± 0.04–2.04 ± 0.04 M$\odot$ and 12.66 ± 0.39–13.41 ± 0.71 km for BSRV's parameter sets, respectively. The value of $\Lambda_{1.4}$ which lie in the range 525.84 ± 151.48–682.57 ± 219.73 for BSRV's parametrization also satisfies the GW170817 event [15,71] and constraints obtained using Bayesian analysis and PREX-II reported in Refs. [26,70,71]. Covariance analysis to measure the accuracy of the model parameters is also performed. This enabled us to estimate the statistical uncertainties in the model parameters along with various correlations amongst the nuclear matter observables and parameters.

CREX and PREX-II data on neutron skin thickness has opened an important new perspective to constrain the density dependence of symmetry energy and energy density functionals and having a considerable effect on the isovector channel. The BSRV-CREX parametrization obtained by incorporating CREX data provides the smaller value of symmetry energy, its slope at saturation density and neutron skin thickness are significantly very small. This may be due to the large value of coupling g_δ which seems to play an important role during the calibration procedure of model parameters and is responsible for soft and stiff behavior of symmetry energy in medium and high density regime. But the radius and tidal deformability of $1.4M_\odot$ neutron star reveals some tension with the revised limit of $\Lambda_{1.4} \leqslant 580$ [15]. The BSRV-PREX parametrization obtained keeping in view the PREX-II data suggests stiff symmetry energy and stiff EoS. For BSRV-PREX and BSRV-CPREX models, the tidal deformability of $1.4M_\odot$ neutron star has some overlap with the revised limit of $\Lambda_{1.4} \leqslant 580$ within 1σ uncertainty reported in Ref. [15]. BSRV-CREX gives soft density dependence of symmetry energy whereas BSRV-PREX and BSRV-CPREX provide its stiff value. The analysis of the present work shows that no consistent conclusion from the theoretical side could be obtained when using recently measured CREX and PREX-II data. We are hoping that novel experimental studies are necessary to resolve this conflict or discrepancies.

[1] J. M. Lattimer, The nuclear equation of state and neutron star masses, Annu. Rev. Nucl. Part. Sci. **62**, 485 (2012).

[2] M. Oertel, M. Hempel, T. Klähn, and S. Typel, Equations of state for supernovae and compact stars, Rev. Mod. Phys. **89**, 015007 (2017).

[3] X. Roca-Maza and N. Paar, Nuclear equation of state from ground and collective excited state properties of nuclei, Prog. Part. Nucl. Phys. **101**, 96 (2018).

[4] J. M. Lattimer and M. Prakash, The physics of neutron stars, Science **304**, 536 (2004).

[5] S. K. Dhiman, R. Kumar, and B. K. Agrawal, Nonrotating and rotating neutron stars in the extended field theoretical model, Phys. Rev. C **76**, 045801 (2007).

[6] V. Thakur, R. Kumar, P. Kumar, V. Kumar, B. K. Agrawal, and S. K. Dhiman, Relativistic mean field model parametrizations in the light of GW170817, GW190814, and PSR j0740+6620, Phys. Rev. C **106**, 025803 (2022).

[7] V. Thakur, R. Kumar, P. Kumar, V. Kumar, M. Kumar, C. Mondal, B. K. Agrawal, and S. K. Dhiman, Effects of an isovector scalar meson on the equation of state of dense matter within a relativistic mean field model, Phys. Rev. C **106**, 045806 (2022).

[8] P. Haensel, A. Y. Potekhin, and D. G. Yakovlev, *Neutron Stars 1: Equation of State and Structure*, Vol. 326 (Springer Science & Business Media, Cham, 2007).

[9] J. M. Lattimer, Neutron stars, Gen. Rel. Grav. **46**, 1713 (2014).

[10] G. Baym, T. Hatsuda, T. Kojo, P. D. Powell, Y. Song, and T. Takatsuka, From hadrons to quarks in neutron stars: A review, Rep. Prog. Phys. **81**, 056902 (2018).

[11] K. Hebeler, J. M. Lattimer, C. J. Pethick, and A. Schwenk, Constraints on Neutron Star Radii Based on Chiral Effective Field Theory Interactions, Phys. Rev. Lett. **105**, 161102 (2010).

[12] K. Hebeler, J. M. Lattimer, C. J. Pethick, and A. Schwenk, Equation of state and neutron star properties constrained by nuclear physics and observation, Astrophys. J. **773**, 11 (2013).

[13] P. B. Demorest, Tim Pennucci, S. M. Ransom, M. S. E. Roberts, and J. W. T. Hessels, A two-solar-mass neutron star measured using Shapiro delay, Nature (London) **467**, 1081 (2010).

[14] J. Antoniadis, P. C. C. Freire, N. Wex, T. M. Tauris, R. S. Lynch, M. H. van Kerkwijk, M. Kramer, C. Bassa, V. S. Dhillon, T. Driebe *et al.*, A massive pulsar in a compact relativistic binary, Science **340**, 1233232 (2013).

[15] B. P. Abbott, R. Abbott, T. D. Abbott, F. Acernese, K. Ackley, C. Adams, T. Adams, P. Addesso, R. X. Adhikari, V. B. Adya *et al.*, GW170817: Measurements of Neutron Star Radii and Equation of State, Phys. Rev. Lett. **121**, 161101 (2018).

[16] B. P. Abbott, R. Abbott, T. D. Abbott, F. Acernese, K. Ackley, C. Adams, T. Adams, P. Addesso, R. X. Adhikari, V. B. Adya *et al.*, Properties of the Binary Neutron Star Merger GW170817, Phys. Rev. X **9**, 011001 (2019).

[17] Z. Arzoumanian, A. Brazier, S. Burke-Spolaor, S. Chamberlin, S. Chatterjee, B. Christy, J. M. Cordes, N. J. Cornish, F. Crawford, H. T. Cromartie *et al.*, The nanograv 11-year data set: High-precision timing of 45 millisecond pulsars, Astrophys. J. Suppl. S. **235**, 37 (2018).

[18] M. C. Miller, F. K. Lamb, A. J. Dittmann, S. Bogdanov, Z. Arzoumanian, K. C. Gendreau, S. Guillot, A. K. Harding, W. C. G. Ho, J. M. Lattimer, R. M. Ludlam, S. Mahmoodifar, S. M. Morsink, P. S. Ray, T. E. Strohmayer, K. S. Wood, T. Enoto, R. Foster, T. Okajima, G. Prigozhin, and Y. Soong, PSR j0030+0451 mass and radius from NICER data and implications for the properties of neutron star matter, Astrophys. J. **887**, L24 (2019).

[19] T. E. Riley, A. L. Watts, S. Bogdanov, P. S. Ray, R. M. Ludlam, S. Guillot, Z. Arzoumanian, C. L. Baker, A. V. Bilous, D. Chakrabarty, K. C. Gendreau, A. K. Harding, W. C. G. Ho, J. M. Lattimer, S. M. Morsink, and T. E. Strohmayer, A NICER view of PSR J0030+0451: Millisecond pulsar parameter estimation, Astrophys. J. Lett. **887**, L21 (2019).

[20] G. Raaijmakers, T. E. Riley, A. L. Watts, S. K. Greif, S. M. Morsink, K. Hebeler, A. Schwenk, T. Hinderer, S. Nissanke, S. Guillot, Z. Arzoumanian, S. Bogdanov, D. Chakrabarty, K. C. Gendreau, W. C. G. Ho, J. M. Lattimer, R. M. Ludlam, and M. T. Wolff, A NICER view of PSR j0030+0451: Implications for the dense matter equation of state, Astrophys. J. **887**, L22 (2019).

[21] D. Adhikari *et al.* (CREX Collaboration), Precision Determination of the Neutral Weak form Factor of ^{48}Ca, Phys. Rev. Lett. **129**, 042501 (2022).

[22] D. Adhikari, H. Albataineh, D. Androic, K. Aniol, D. S. Armstrong, T. Averett, C. A. Gayoso, S. Barcus, V. Bellini, R. S. Beminiwattha *et al.*, Accurate Determination of the Neutron Skin Thickness of ^{208}Pb Through Parity-Violation in Electron Scattering, Phys. Rev. Lett. **126**, 172502 (2021).

[23] P.-G. Reinhard, J. Piekarewicz, W. Nazarewicz, B. K. Agrawal, N. Paar, and X. Roca-Maza, Information content of the weak-charge form factor, Phys. Rev. C **88**, 034325 (2013).

[24] P.-G. Reinhard, X. Roca-Maza, and W. Nazarewicz, Information Content of the Parity-Violating Asymmetry in ^{208}Pb, Phys. Rev. Lett. **127**, 232501 (2021).

[25] P.-G. Reinhard, X. Roca-Maza, and W. Nazarewicz, Combined Theoretical Analysis of the Parity-Violating Asymmetry for ^{48}Ca and ^{208}Pb, Phys. Rev. Lett. **129**, 232501 (2022).

[26] B. T. Reed, F. J. Fattoyev, C. J. Horowitz, and J. Piekarewicz, Implications of PREX-2 on the Equation of State of Neutron-Rich Matter, Phys. Rev. Lett. **126**, 172503 (2021).

[27] H. T. Cromartie, E. Fonseca, S. M. Ransom, P. B. Demorest, Z. Arzoumanian, H. Blumer, P. R. Brook, M. E. DeCesar, T. Dolch, J. A. Ellis, R. D. Ferdman, E. C. Ferrara, N. Garver-Daniels, P. A. Gentile, M. L. Jones, M. T. Lam, D. R. Lorimer, R. S. Lynch, M. A. McLaughlin, C. Ng, D. J. Nice, T. T. Pennucci, R. Spiewak, I. H. Stairs, K. Stovall, J. K. Swiggum, and W. W. Zhu, Relativistic Shapiro delay measurements of an extremely massive millisecond pulsar, Nature Astronomy **4**, 72 (2020).

[28] P. Danielewicz, Determination of the equation of state of dense matter, Science **298**, 1592 (2002).

[29] R. Kumar, B. K. Agrawal, and S. K. Dhiman, Effects of ω meson self-coupling on the properties of finite nuclei and neutron stars, Phys. Rev. C **74**, 034323 (2006).

[30] N. K. Glendenning, *Compact Stars: Nuclear Physics, Particle Physics, and General Relativity* (Springer-Verlag, New York, 2000).

[31] T. J. Bürvenich, D. G. Madland, and P.-G. Reinhard, Adjustment studies in self-consistent relativistic mean-field models, Nucl. Phys. A **744**, 92 (2004).

[32] S. Kirkpatrick, Optimization by simulated annealing: Quantitative studies, J. Stat. Phys. **34**, 975 (1984).

[33] J. Dobaczewski, W. Nazarewicz, and P. G. Reinhard, Error estimates of theoretical models: A guide, J. Phys. G: Nucl. Part. Phys. **41**, 074001 (2014).

[34] W.-C. Chen and J. Piekarewicz, Searching for isovector signatures in the neutron-rich oxygen and calcium isotopes, Phys. Lett. B **748**, 284 (2015).

[35] C. Mondal, B. K. Agrawal, and J. N. De, Constraining the symmetry energy content of nuclear matter from nuclear masses: A covariance analysis, Phys. Rev. C **92**, 024302 (2015).

[36] F. J. Fattoyev and J. Piekarewicz, Accurate calibration of relativistic mean-field models: Correlating observables and providing meaningful theoretical uncertainties, Phys. Rev. C **84**, 064302 (2011).

[37] S. Brandt, *Statistical and Computational Methods in Data Analysis* (Springer, Berlin, 1997).

[38] P.-G. Reinhard and W. Nazarewicz, Information content of a new observable: The case of the nuclear neutron skin, Phys. Rev. C **81**, 051303(R) (2010).

[39] M. Wang, W. J. Huang, F. G. Kondev, G. Audi, and S. Naimi, The AME 2020 atomic mass evaluation (II): Tables, graphs, and references, Chin. Phys. C **45**, 030003 (2021).

[40] I. Angeli and K. P. Marinova, Table of experimental nuclear ground state charge radii: An update, At. Data Nucl. Data Tables **99**, 69 (2013).

[41] G. A. Lalazissis, J. König, and P. Ring, New parametrization for the Lagrangian density of relativistic mean field theory, Phys. Rev. C **55**, 540 (1997).

[42] B. Kumar, S. K. Patra, and B. K. Agrawal, New relativistic effective interaction for finite nuclei, infinite nuclear matter, and neutron stars, Phys. Rev. C **97**, 045806 (2018).

[43] F. J. Fattoyev, C. J. Horowitz, J. Piekarewicz, and B. Reed, Gw190814: Impact of a 2.6 solar mass neutron star on the nucleonic equations of state, Phys. Rev. C **102**, 065805 (2020).

[44] L. Rezzolla, E. R. Most, and L. R. Weih, Using gravitational-wave observations and quasi-universal relations to constrain the maximum mass of neutron stars, Astrophys. J. Lett. **852**, L25 (2018).

[45] P. Ring and P. Schuck, *The Nuclear Many-body Problem*, Texts and Monographs in Physics (Springer-Verlag, New York, Heidelberg, Berlin, 1980).

[46] S. Karatzikos, A. V. Afanasjev, G. A. Lalazissis, and P. Ring, The fission barriers in actinides and superheavy nuclei in covariant density functional theory, Phys. Lett. B **689**, 72 (2010).

[47] T. Duguet, P. Bonche, P.-H. Heenen, and J. Meyer, Pairing correlations. II. Microscopic analysis of odd-even mass staggering in nuclei, Phys. Rev. C **65**, 014311 (2001).

[48] C. Mondal, B. K. Agrawal, J. N. De, and S. K. Samaddar, Sensitivity of elements of the symmetry energy of nuclear matter to the properties of neutron-rich systems, Phys. Rev. C **93**, 044328 (2016).

[49] C. D. Pruitt, R. J. Charity, L. G. Sobotka, M. C. Atkinson, and W. H. Dickhoff, Systematic Matter and Binding-Energy Distributions from a Dispersive Optical Model Analysis, Phys. Rev. Lett. **125**, 102501 (2020).

[50] J. Jastrzebski, A. Trzcinska, P. Lubiski, B. Kos, F. J. Hartmann, T. v. Egidy, and S. Wycech, Neutron density distributions from antiprotonic atoms compared with hadron scattering data, Int. J. Mod. Phys. E **13**, 343 (2004).

[51] A. Trzcinska, J. Jastrzebski, P. Lubinski, F. J. Hartmann, R. Schmidt, T. Von Egidy, and B. Klos, Neutron Density Distributions Deduced from Antiprotonic Atoms, Phys. Rev. Lett. **87**, 082501 (2001).

[52] E. Yüksel and N. Paar, Implications of parity-violating electron scattering experiments on 48ca (CREX) and ^{208}Pb (PREX-II) for nuclear energy density functionals, Phys. Lett. B **836**, 137622 (2023).

[53] B.-A. Li and X. Han, Constraining the neutron–proton effective mass splitting using empirical constraints on the density dependence of nuclear symmetry energy around normal density, Phys. Lett. B **727**, 276 (2013).

[54] G. Colo, U. Garg, and H. Sagawa, Symmetry energy from the nuclear collective motion: Constraints from dipole, quadrupole, monopole, and spin-dipole resonances, Eur. Phys. J. A **50**, 26 (2014).

[55] J. Piekarewicz, Symmetry energy constraints from giant resonances: A relativistic mean-field theory overview, Eur. Phys. J. A **50**, 25 (2014).

[56] J. Zimmerman, Z. Carson, K. Schumacher, A. W. Steiner, and K. Yagi, Measuring nuclear matter parameters with NICER and LIGO/Virgo, arXiv:2002.03210.

[57] A. W. Steiner, J. M. Lattimer, and E. F. Brown, The equation of state from observed masses and radii of neutron stars, Astrophys. J. **722**, 33 (2010).

[58] T. Maruyama and S. Chiba, Equation of state of neutron-star matter and the isovector nucleon optical model potential, J. Phys. G: Nucl. Part. Phys. **25**, 2361 (1999).

[59] J. R. Oppenheimer and G. M. Volkoff, On massive neutron cores, Phys. Rev. **55**, 374 (1939).

[60] R. C. Tolman, Static solutions of einstein's field equations for spheres of fluid, Phys. Rev. **55**, 364 (1939).

[61] E. Fonseca, T. T. Pennucci, J. A. Ellis, I. H. Stairs, D. J. Nice, S. M. Ransom, P. B. Demorest, Z. Arzoumanian, K. Crowter, T. Dolch *et al.*, The nanograv nine-year data set: Mass and geometric measurements of binary millisecond pulsars, Astrophys. J. **832**, 167 (2016).

[62] T. E. Riley, A. L. Watts, P. S. Ray, S. Bogdanov, S. Guillot, S. M. Morsink, A. V. Bilous, Z. Arzoumanian, D. Choudhury, J. S. Deneva *et al.*, A nicer view of the massive pulsar PSR j0740+ 6620 informed by radio timing and XMM-Newton spectroscopy, Astrophys. J. Lett. **918**, L27 (2021).

[63] M. C. Miller, F. K. Lamb, A. J. Dittmann, S. Bogdanov, Z. Arzoumanian, K. C. Gendreau, S. Guillot, W. C. G. Ho, J. M. Lattimer, M. Loewenstein *et al.*, The radius of PSR J0740 + 6620 from NICER and XMM-Newton data, Astrophys. J. Lett. **918**, L28 (2021).

[64] G. Baym, C. Pethick, and P. Sutherland, The ground state of matter at high densities: Equation of state and stellar models, Astrophys. J. **170**, 299 (1971).

[65] E. Annala, T. Gorda, A. Kurkela, and A. Vuorinen, Gravitational-Wave Constraints on the Neutron-Star-Matter Equation of State, Phys. Rev. Lett. **120**, 172703 (2018).

[66] T. Hinderer, Tidal love numbers of neutron stars, Astrophys. J. **677**, 1216 (2008).

[67] T. Hinderer, B. D. Lackey, R. N. Lang, and J. S. Read, Tidal deformability of neutron stars with realistic equations of state and their gravitational wave signatures in binary inspiral, Phys. Rev. D **81**, 123016 (2010).

[68] T. Hinderer, Tidal love numbers of neutron stars, Astrophys. J. **697**, 964 (2009).

[69] T. Damour and A. Nagar, Effective one body description of tidal effects in inspiralling compact binaries, Phys. Rev. D **81**, 084016 (2010).

[70] Y. Li, H. Chen, D. Wen, and J. Zhang, Constraining the nuclear symmetry energy and properties of the neutron star from GW170817 by Bayesian analysis, Eur. Phys. J. A **57**, 31 (2021).

[71] B. P. Abbott, R. Abbott, T. D. Abbott, F. Acernese, K. Ackley, C. Adams, T. Adams, P. Addesso, R. X. Adhikari, V. B. Adya *et al.*, GW170817: Observation of Gravitational Waves from a Binary Neutron Star Inspiral, Phys. Rev. Lett. **119**, 161101 (2017).